ChemComm

COMMUNICATION

View Article Online
View Journal | View Issue



Cite this: *Chem. Commun.*, 2021, **57**, 4122

Received 11th January 2021,
Accepted 23rd March 2021

DOI: 10.1039/d1cc00185j

rsc.li/chemcomm



# A [$Mn_{18}$] wheel-of-wheels†

Marco Coletta,[a] Thomais G. Tziotzi,[b] Mark Gray,[a] Gary S. Nichol,[a] Mukesh K. Singh,*[a] Constantinos J. Milios*[b] and Euan K. Brechin*[a]

**A [$Mn_{18}$] wheel of wheels is obtained from the reaction of $MnBr_2{\cdot}4H_2O$ and $LH_3$ in MeOH. The metallic skeleton reveals two asymmetric [$Mn^{III}_6Mn^{II}_2$] square wheels connected into a larger wheel *via* two $Mn^{II}$ ions. Magnetic susceptibility and magnetisation data reveal competing exchange interactions, supported by computational studies.**

Beyond beautiful structural aesthetics, wheels of paramagnetic metal ions have proven to be vital for revealing quantum effects,[1] constructing very high spin molecules,[2] engineering toroidal magnetic moments,[3] developing magnetic Möbius strips,[4] understanding frustration effects,[5] probing slow magnetisation relaxation,[6] investigating quantum information processing,[7] and developing magneto–structural correlations.[8] In Mn coordination chemistry wheels have presented nuclearities as large as eighty-four,[9] displaying a variety of topologies constructed from chains of single metal ions and polymetallic building blocks.[10–13] Amongst ligand types, those containing one or more ethanolamine (eaH) moieties (Fig. 1) have proven enormously successful in building a breadth of structurally and magnetically fascinating species.[14] Herein we extend this body of work to include the ligand 1,3,5-tri(2-hydroxyethyl)-1,3,5-triazacyclohexane ($LH_3$), which contains three linked eaH units. A search of the Cambridge Structural Database reveals just four hits in 3d transition metal chemistry. The first was the monomer [$Cr(CO)_3(LH_3)$],[15] the second an aesthetically pleasing [$Mn_{16}$] complex in which the ligand was generated serendipitously *in situ*,[16] and the third and fourth structurally related [$Mn_{16}$] and [$Mn_{10}$] square wheels.[17]

Reaction of $MnBr_2{\cdot}4H_2O$ with $LH_3$ in MeOH affords black crystals of [$Mn^{III}_{12}Mn^{II}_6(O)_6(OH)_2(OMe)_6(L)_4(LH)_2Br_{12}$] (**1**, Fig. 2 and Fig. S1, ESI†) after 2 days (see ESI† for full experimental details).

Compound **1** crystallises in the monoclinic space group *I*2/*a*, with half the complex in the asymmetric unit. The metallic skeleton of **1** describes two distorted 'square' [$Mn^{III}_6Mn^{II}_2$] wheels (Mn1–7) linked *via* two $Mn^{II}$ ions (Mn8). The wheels comprise four vertex-sharing [$Mn_3$] triangles (Fig. 3). Pertinent bond lengths and angles are provided in Table S1 (ESI†).

The [$Mn^{III}_6Mn^{II}_2(\mu_3\text{-}O)_6(\mu\text{-}OH)_2(OMe)_6$] core of the square wheel is asymmetric (Fig. 2 and 3). Three of the four corners (Mn1–3, Mn3–5, Mn5–7) are bridged 'internally' *via* a 'T-shaped' $\mu_3\text{-}O^{2-}$ ion (O11–O13) and two externally *via* a $\mu\text{-}OMe^-$ ion (Mn1–O15–Mn2, Mn6–O16–Mn7). The fourth corner (Mn1, Mn7, Mn9) is connected only 'internally' *via* one $\mu_3\text{-}OMe^-$ ion (O14) and one $\mu\text{-}OH^-$ ion (O10). The $Mn^{II}$ ions (Mn4, Mn9) occupy opposite vertices in the square. There are two $\mu_6\text{-}L^{3-}$ and one $\mu_5\text{-}LH^{2-}$ ligands in the asymmetric unit (Fig. 3). The former both sit above a [$Mn^{III}_3$] triangle which acts as the corner of the square, with each of the three N atoms coordinated to a different $Mn^{III}$ ion. The O-atoms also bond to the same metal ions but further μ-bridge to a neighbouring $Mn^{II}$ ion in the square. The dianionic $LH^{2-}$ ligands sit above

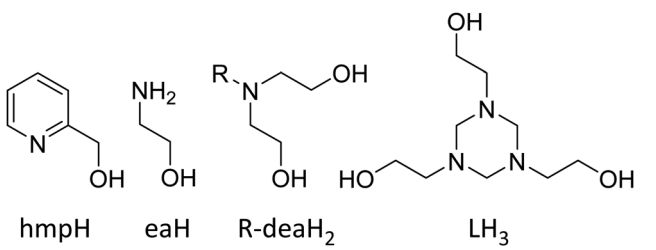


**Fig. 1** The N,O-chelates 2-(hydroxymethyl)pyridine (hmpH), ethanolamine (eaH), di- and triethanolamine (R-deaH$_2$; R = alkyl, $CH_2CH_2OH$, respectively), and 1,3,5-tri(2-hydroxyethyl)-1,3,5-triazacyclohexane ($LH_3$), all of which contain one or more linked ethanolamine moieties.

[a] *EaStCHEM School of Chemistry, The University of Edinburgh, David Brewster Road, Edinburgh, EH9 3FJ, UK. E-mail: E.Brechin@ed.ac.uk, mklsingh36@gmail.com*
[b] *Department of Chemistry, The University of Crete, Voutes, 71003, Herakleion, Greece. E-mail: komil@uoc.gr*

† Electronic supplementary information (ESI) available: Full experimental procedures, crystallographic data, magnetic data and additional figures. CCDC 2054790. For ESI and crystallographic data in CIF or other electronic format see DOI: 10.1039/d1cc00185j

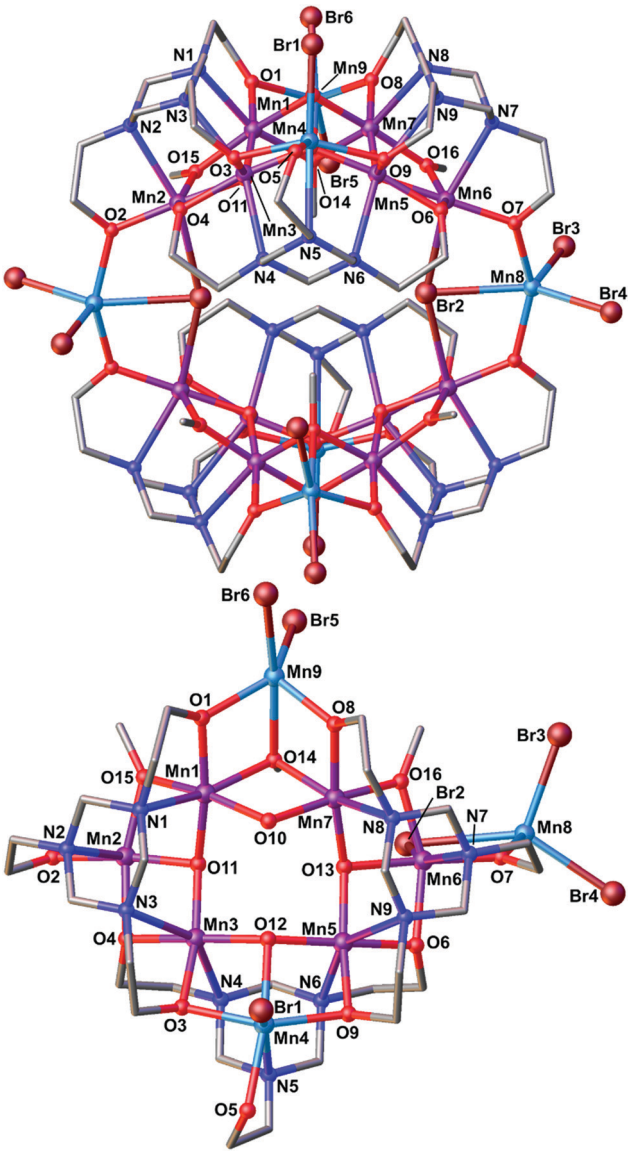


Fig. 2 The molecular structure (top) and asymmetric unit (bottom) of **1**. Colour code: $Mn^{III}$ = purple, $Mn^{II}$ = light blue, O = red, N = dark blue, C = grey, Br = brown. H atoms omitted for clarity.

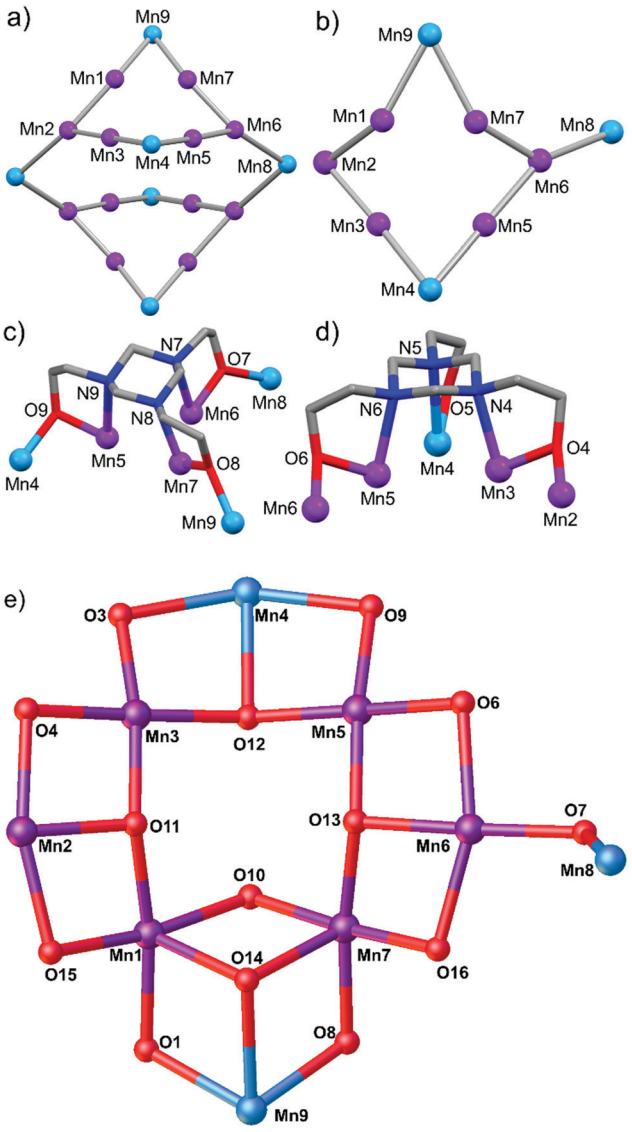


Fig. 3 Metallic skeleton of (a) **1**, and (b) the asymmetric unit of **1**, highlighting the square wheel and the linking of the two square wheels. The coordination modes of (c) the two $\mu_6$-$L^{3-}$ and (d) one $\mu_5$-$LH^{2-}$ ligands in the asymmetric unit. (d) metal–oxygen core of the asymmetric unit. Colour code as Fig. 2.

the $[Mn^{III}_2Mn^{II}]$ triangle (Mn3–5) with each N-atom (N4–6) coordinated to a different Mn ion. Two of the three O-arms (O4, O6) μ-bridge to a neighbouring $Mn^{III}$ ion in the square, with the third O-arm (O5) terminally bonded to a $Mn^{II}$ ion.

The two $\mu_3$-$Br^-$ ions (Br2 and symmetry equivalent) are bonded to the $Mn^{II}$ ions (Mn8) that link the two halves of the cluster together, also bridging between Mn2 and Mn6 (Fig. 1). Mn8 is 5-coordinate and in trigonal bipyramidal geometry, its $\{MnO_2Br_3\}$ coordination sphere being completed with two monodentate Br ions. Mn9 is coordinated in a similar fashion, but Mn4 is square pyramidal and bonded to just one Br ion and possesses a $\{MnO_4Br\}$ coordination sphere (Fig. S2, ESI†). Thus, the $Mn^{II}$ sites are easily distinguished by all being bonded to Br ions. The six $Mn^{III}$ ions in the asymmetric unit (Mn1–3, Mn5–7) are all in Jahn–Teller (JT) elongated octahedral geometries (Fig. S2, S3 and Table S2, ESI†), which are also easily distinguished since they all involve the triazacyclohexane ring N-heteroatoms.

The closest inter-molecular interactions occur between the terminally bonded Br ions and the C-atoms of the triazacyclohexane ring (C···N ≥ 3.85 Å) directing the formation of columns of **1** in the extended structure along the *a*-axis of the cell (Fig. S4, ESI†). A search of the Cambridge Structural Database reveals that seventeen $[Mn_{18}]$ clusters have been reported previously, but none have the topology seen in **1**. We note that there are clear structural similarities to the $[Mn_{16}]$ and $[Mn_{10}]$ clusters we recently reported with this ligand, both of which describe square, wheel-like structures built from $[Mn_3]$ triangular building blocks as directed by the coordination of the triazatriol ligand.[17]

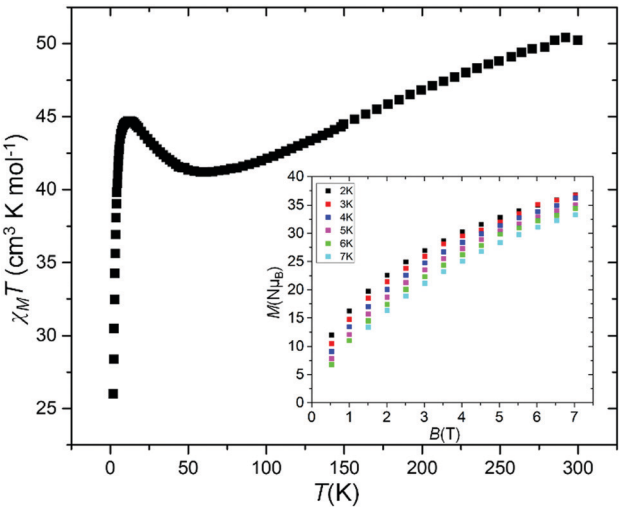


Fig. 4 Temperature dependence of the $\chi_M T$ product for **1** collected in an applied magnetic field of $B$ = 0.5 T. The inset shows the VTVB magnetisation data in the temperature/field ranges 2–7 K/0.5–7 T.

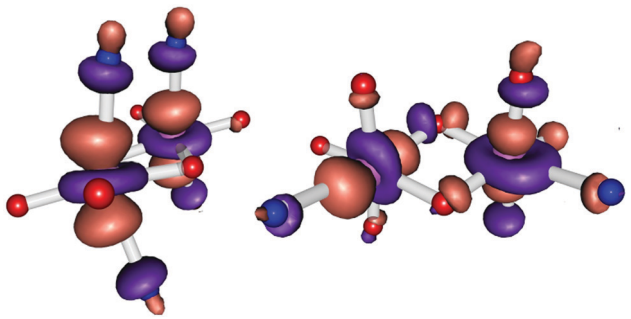

Fig. 5 Schematic presentation of the Jahn–Teller axis for (left) {Mn5–Mn6, $J_1$} and (right) {Mn1–Mn7, $J_3$}. For $J_1$ the JT axes of the $Mn^{III}$ ions are found to be collinear and perpendicular to the bridging plane of the dimer (Type I). For $J_3$ the JT axes of the $Mn^{III}$ ions are perpendicular to each other with one lying parallel to the bridging plane and the other perpendicular to the bridging plane (type III).

The magnetic properties of a freshly prepared polycrystalline sample of **1** were measured in an applied field, $B$ = 0.5 T, over the $T$ = 2–300 K temperature range. The experimental results are shown in Fig. 4, in the form of the $\chi_M T$ product, where $\chi_M = M/B$, and $M$ is the magnetisation of the sample. At room temperature the $\chi_M T$ product of **1** (50.43 cm$^3$ K mol$^{-1}$) is lower than the sum of the Curie constants expected for a [$Mn^{III}_{12}Mn^{II}_6$] (62.25 cm$^3$ K mol$^{-1}$) unit. As temperature decreases, $\chi_M T$ first decreases to a value of 41.20 cm$^3$ K mol$^{-1}$ at $T$ = 60 K, before increasing to a maximum of 44.70 cm$^3$ K mol$^{-1}$ at 11 K, and then falls to a value of 26.00 cm$^3$ K mol$^{-1}$ at $T$ = 2 K. This behaviour is clearly indicative of competing exchange interactions, with the increase between 60–11 K perhaps suggestive of ferromagnetic exchange between the two square [$Mn^{III}_6Mn^{II}_2$] wheels. The decrease in $\chi_M T$ at the lowest temperatures is attributed to a combination of intra- and intermolecular antiferromagnetic exchange and zero field splitting (*zfs*) effects.

Low temperature variable-temperature-and-variable-field (VTVB) magnetisation data were measured in the temperature range 2–7 K, in magnetic fields up to 7.0 T (Fig. 4, inset and Fig. S5, ESI†). At the lowest temperature and highest field measured, $M$ reaches a value of $\sim$37 $\mu_B$ but does not saturate. There are no out-of-phase signals in ac susceptibility measurements in zero dc field.

Since the nuclearity of **1** precludes a fit of the experimental data *via* standard techniques, we have calculated the magnetic exchange interactions using computational tools known to accurately reproduce experimental $J$ values (see the Computational Details section in the ESI† for more details).[18] We have performed calculations on a model complex, **1a**, which is simply the asymmetric unit, *i.e.* one [$Mn^{III}_6Mn^{II}_2$] square wheel plus one linking $Mn^{II}$ ion (Fig. S6, ESI†). Based on symmetry and the different bridging groups/angles present, the number of unique magnetic exchange interactions can be reduced to six (Table S3 and Fig. S7, ESI†). These are: ($J_1$) $Mn^{III}$–$Mn^{III}$ mediated through $\mu_3$-$O^{2-}$ and μ-OR; ($J_2$) $Mn^{III}$–$Mn^{III}$ mediated through $\mu_3$-$O^{2-}$; ($J_3$) $Mn^{III}$–$Mn^{III}$ mediated through μ-OH and $\mu_3$-OR; ($J_4$) $Mn^{II}$–$Mn^{III}$ mediated through $\mu_3$-$O^{2-}$ and μ-OR; ($J_5$) $Mn^{II}$–$Mn^{III}$ mediated through μ-OR and $\mu_3$-OR; and ($J_6$) $Mn^{II}$–$Mn^{III}$ mediated through μ-Br and μ-OR.

The first two interactions ($J_1$ and $J_2$) are found to be antiferromagnetic, whereas the remaining four interactions ($J_3$–$J_6$) are estimated to be ferromagnetic (Table S3 and Fig. S8, ESI†). For the $J_1$ interaction, the JT axis of both $Mn^{III}$ ions are found to be collinear and perpendicular to the bridging plane of the dimer (Fig. 5 and Fig. S9a, ESI†). According to the magnetostructural correlation for [$Mn^{III}_2$] dimers discussed in ref. 19 this describes a Type I geometry that should lead to antiferromagnetic exchange.[19] Overlap integral ($|S_{ab}|$) calculations (Table S4, ESI†) are in agreement, with two strong and four intermediate interactions detected, leading to a relatively strong antiferromagnetic interaction, $J_1$ = −10 cm$^{-1}$ (Fig. S10a–f, ESI†). For the $J_2$ interaction, the $Mn^{III}$ ions are bridged *via* $\mu_3$-$O^{2-}$ ions with Mn–$\mu_3$O–Mn angles between 132–136°. Overlap calculations suggest one strong and four intermediate interactions (Fig. S10g–k, ESI†), leading to a relatively strong antiferromagnetic interaction, $J_2$ = −9 cm$^{-1}$.

For the $J_3$–$J_6$ interactions, overlap integral calculations reveal that only intermediate interactions are observed, resulting in ferromagnetic exchange coupling with $J_3$ = +8 cm$^{-1}$, $J_4$ = +1 cm$^{-1}$, $J_5$ = +2 cm$^{-1}$ and $J_6$ = +2 cm$^{-1}$ (Fig. S10l–w, ESI†). These values are in-line with those previously reported for similar bridging moieties, and consistent with published magnetostructral studies.[20] The magnitude and sign of the magnetic exchange interactions can also be related to the calculated average total overlap integral ($\sum|S_{a(3d)b(3d)}|/n$, Fig. S11, ESI†).[21] The smaller the average total overlap integral, the larger the ferromagnetic interaction (or the smaller the antiferromagnetic interaction) and *vice versa*. Note that for the $J_3$ interaction, the JT axes of the $Mn^{III}$ ions lie perpendicular to each other, with one lying parallel to the bridging plane and the other perpendicular to the bridging plane. This is a Type III geometry (Fig. 5 and Fig. S9b, ESI†), and would be expected to promote ferromagnetic exchange.[19] The $J_1$–$J_4$ interactions between $Mn^{III/II}$–$Mn^{III}$ centres are also mediated *via*

 

the $(R_2)N–CH_2–N(R_2)$ group of the triazatriol ligand, however the expected contribution to the total magnetic exchange through this long bridging group would be expected to be minimal. Indeed the calculated spin density on the connecting $–CH_2–$ group is close to zero ($\leq 0.003$, Fig. S12, ESI†) breaking any spin delocalisation/polarisation pathway. A summary of these results is shown in Fig. S8 (ESI†) alongside a cartoon of the "spin-up"/"spin-down" orientations of the individual Mn ions in **1a**.

In summary, the reaction between $MnBr_2{\cdot}4H_2O$ with $LH_3$ in MeOH affords the species $[Mn^{III}_{12}Mn^{II}_6(O)_6(OH)_2(OMe)_6(L)_4(LH)_2Br_{12}]$, **1**. The metal core of **1** consists of two square $[Mn^{III}_6Mn^{II}_2]$ wheels linked *via* two $Mn^{II}$ ions. The wheels incorporate four vertex sharing triangles, which leads to competing exchange interactions, while the link between wheels is ferromagnetic. Future work on a larger library of Mn-based triazatriol complexes will look to develop magneto-structural studies incorporating theoretical calculations in tandem with methodologies capable of simulating the magnetic data of such sizeable species.[22] We speculate that full deprotonation and the conversion of the hydroxides to oxides may lead to a more symmetric wheel, or wheel of wheels, while oxidation of the $Mn^{II}$ ions should also result in significant structural rearrangement. It is also interesting to note that in all the Mn complexes we have isolated with $LH_3$ thus far[17] – $[Mn_{10}]$, $[Mn_{16}]$ and $[Mn_{18}]$ – the direction of the JT axes of the $Mn^{III}$ ions is dictated by the triaza N-atoms (*i.e.* perpendicular to the triaza macrocycle). This has important consequences for controlling nearest neighbour magnetic exchange interactions and thus needs to be carefully considered in future design strategies.

We thank the EPSRC for financial support under grant reference numbers EP/N01331X/1, and the Marie Skłodowska-Curie actions (MSCA) for grant MMQIP 832488 (to MKS). Crystallographic data for 1 were measured remotely at beam line I-19 of Diamond Light Source (award CY22240). CJM and TGT thank the Hellenic Foundation for Research and Innovation (H.F.R.I.) under the "First Call for H.F.R.I. Research Projects to support Faculty members and Researchers and the procurement of high-cost research equipment grant" (Project Number: 400). This work has made use of the resources provided by the Edinburgh Compute and Data Facility (ECDF) (http://www.ecdf.ed.ac.uk/).

## Conflicts of interest

There are no conflicts to declare.

## Notes and references

1 K. L. Taft, C. D. Delfs, G. C. Papaefthymiou, S. Foner, D. Gatteschi and S. J. Lippard, *J. Am. Chem. Soc.*, 1994, **116**, 823–832.
2 A. Baniodeh, N. Magnani, Y. Lan, G. Buth, C. E. Anson, J. Richter, M. Affronte, J. Schnack and A. K. Powell, *npj Quantum Mater.*, 2018, **3**, 10.
3 L. Ungur, S. K. Langley, T. N. Hooper, B. Moubaraki, E. K. Brechin, K. S. Murray and L. F. Chibotaru, *J. Am. Chem. Soc.*, 2012, **134**, 18554–18557.
4 O. Cador, D. Gatteschi, R. Sessoli, F. K. Larsen, J. Overgaard, A.-L. Barra, S. J. Teat, G. A. Timco and R. E. P. Winpenny, *Angew. Chem., Int. Ed.*, 2004, **43**, 5196–5200.
5 M. L. Baker, G. A. Timco, S. Piligkos, J. S. Mathiesone, H. Mutka, F. Tuna, P. Kozłowskif, M. Antkowiakf, T. Guidi, T. Gupta, H. Rath, R. J. Woolfson, G. Kamieniarz, R. G. Pritchard, H. Weihe, L. Cronin, G. Rajaraman, D. Collison, E. J. L. McInnes and R. E. P. Winpenny, *Proc. Natl. Acad. Sci. U. S. A.*, 2012, **109**, 19113–19118.
6 S. J. Shah, C. M. Ramsey, K. J. Heroux, J. R. O'Brien, A. G. DiPasquale, A. L. Rheingold, E. del Barco and D. N. Hendrickson, *Inorg. Chem.*, 2008, **47**, 6245–6253.
7 G. A. Timco, T. B. Faust, F. Tuna and R. E. P. Winpenny, *Chem. Soc. Rev.*, 2011, **40**, 3067–3075.
8 H. W. L. Fraser, G. S. Nichol, D. Uhrín, U. G. Nielsen, M. Evangelisti, J. Schnack and E. K. Brechin, *Dalton Trans.*, 2018, **47**, 15530–15537.
9 A. J. Tasiopoulos, A. Vinslava, W. Wernsdorfer, K. A. Abboud and G. Christou, *Angew. Chem., Int. Ed.*, 2004, **43**, 2117–2121.
10 C. Papatriantafyllopoulou, E. E. Moushi, G. Christou and A. J. Tasiopoulos, *Chem. Soc. Rev.*, 2016, **45**, 1597–1628.
11 M. Manoli, R. Inglis, S. Piligkos, L. Yanhua, W. Wernsdorfer, E. K. Brechin and A. J. Tasiopoulos, *Chem. Commun.*, 2016, **52**, 12829–12832.
12 S. Zartilas, C. Papatriantafyllopoulou, T. C. Stamatatos, V. Nastopoulos, E. Cremades, E. Ruiz, G. Christou, C. Lampropoulos and A. J. Tasiopoulos, *Inorg. Chem.*, 2013, **52**, 12070–12079.
13 M. Manoli, R. Inglis, M. J. Manos, V. Nastopoulos, W. Wernsdorfer, E. K. Brechin and A. J. Tasiopoulos, *Angew. Chem., Int. Ed.*, 2011, **50**, 4441–4444.
14 A. J. Tasiopoulos and S. P. Perlepes, *Dalton Trans.*, 2008, 5537–5555.
15 M. V. Baker, D. H. Brown, B. W. Skelton and A. H. White, *J. Chem. Soc., Dalton Trans.*, 1999, 1483–1490.
16 M. Riaz, R. K. Gupta, H.-F. Su, Z. Jagličić, M. Kurmoo, C.-H. Tung, D. Sun and L.-S. Zheng, *Inorg. Chem.*, 2019, **58**, 14331–14337.
17 T. G. Tziotzi, M. Coletta, M. Gray, C. L. Campbell, S. J. Dalgarno, G. Lorusso, M. Evangelisti, E. K. Brechin and C. J. Milios, *Inorg. Chem. Front.*, 2021, DOI: 10.1039/D0QI01495H.
18 (*a*) M. K. Singh and G. Rajaraman, *Inorg. Chem.*, 2019, **58**, 3175–3188; (*b*) C. McDonald, S. Sanz, E. K. Brechin, M. K. Singh, G. Rajaraman, D. Gaynor and L. F. Jones, *RSC Adv.*, 2014, **4**, 38182; (*c*) A. E. Dearle, D. J. Cutler, H. W. L. Fraser, S. Sanz, E. Lee, S. Dey, I. F. Diaz-Ortega, G. S. Nichol, H. Nojiri, M. Evangelisti, G. Rajaraman, J. Schnack, L. Cronin and E. K. Brechin, *Angew. Chem., Int. Ed.*, 2019, **58**, 16903–16906.
19 N. Berg, T. Rajeshkumar, S. M. Taylor, E. K. Brechin, G. Rajaraman and L. F. Jones, *Chem. – Eur. J.*, 2012, **18**, 5906.
20 (*a*) R. Maurice, C. de Graaf and N. Guihéry, *J. Chem. Phys.*, 2010, **133**, 084307; (*b*) K. R. Vignesh, S. K. Langley, C. J. Gartshore, B. Moubaraki, K. S. Murray and G. Rajaraman, *Inorg. Chem.*, 2017, **56**, 1932–1949; (*c*) K. R. Vignesh, S. K. Langley, C. J. Gartshore, I. Borilović, C. M. Forsyth, G. Rajaraman and K. S. Murray, *Dalton Trans.*, 2018, **47**, 11820–11833; (*d*) K. R. Vignesh, S. K. Langley, K. S. Murray and G. Rajaraman, *Chem. – Eur. J.*, 2015, **21**, 2881–2892.
21 M. Coletta, S. Sanz, D. J. Cutler, S. J. Teat, K. J. Gagnon, M. K. Singh, E. K. Brechin and S. J. Dalgarno, *Dalton Trans.*, 2020, **49**, 14790–14797.
22 W.-P. Chen, J. Singleton, L. Qin, A. Camón, L. Engelhardt, F. Luis, R. E. P. Winpenny and Y.-Z. Zheng, *Nat. Commun.*, 2018, **9**, 2107.